Article

High On/Off Ratio Carbon Quantum Dot–Chitosan Biomemristors with Coplanar Nanogap Electrodes

Niloufar Raeis-Hosseini,* Dimitra G. Georgiadou, and Christos Papavassiliou

Read Online

ACCESS | Metrics & More | Article Recommendations | Supporting Information

ABSTRACT: A carbon-based natural nanocomposite material comprising carbon quantum dots (CQDs) is dispersed in a chitosan matrix. The CQD−chitosan nanocomposite serves as a solid polymer electrolyte layer of a biomemristor with a Au/CQD−chitosan/Al structure. The active layer of the CQD−chitosan nanocomposite is deposited from its solution on top of coplanar asymmetric nanogap (∼15 nm) Al−Au electrodes, patterned via adhesion lithography. The CQD−chitosan biomemristor presents a high on/off ratio (>10⁶) and reproducible and reliable bipolar resistive switching behavior. An endurance of 160 cycles was recorded, while the high and low resistance states remained stable for more than 10^4 s. This study highlights the potential of both the CQD−chitosan material and nanogap electrode structures for application in nanoscale biocompatible memory devices.

KEYWORDS: biocompatible polymer, biomemristor, resistive switching memory, carbon quantum dots, chitosan
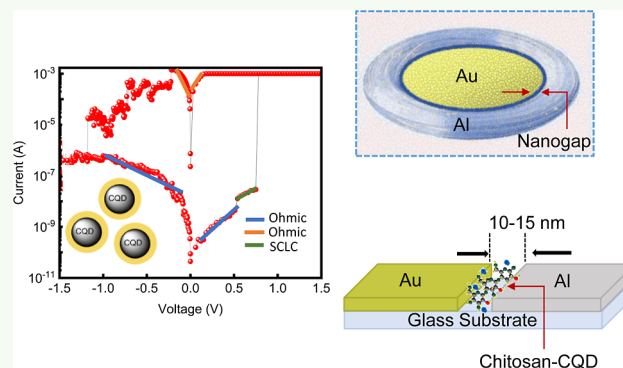
1. INTRODUCTION

A memristor (memory-resistor) is a non-linear resistive switching random access memory device (ReRAM) that has attracted significant attention because of its potential applications ranging from nonvolatile memory[1] to neuromorphic[2] and hybrid edge computing architectures.[3,4] It has emerged as a potential building block of novel storage systems, bionic neural networks,[5] and integrated circuits[6] due to its resistive switching (RS) characteristics. Among the various technologies of nonvolatile memory devices, including magnetic[7] and phase change[8−10] memory systems, a resistive (ReRAM) or memristive device is attractive as it holds promise to resolve the scalability[11,12] and power consumption[13] issues. A memristor (or ReRAM), with its fast switching speed,[14] multilevel data storage,[15] and low power consumption,[16] provides an exceptional platform for the next generation of nanoelectronics.[17]

Numerous materials, including inorganic,[18,19] organic,[20] and hybrid nanocomposites,[21] have been utilized in memristive systems. Biomolecules have an excellent potential to be engaged in producing cost-effective memories due to their non-toxicity, environmentally benign nature, compatibility with various flexible substrates, natural abundance, and ease of fabrication. A memristive device that comprises biocompatible materials as the active layer is called a biomemristor. Utilizing natural materials can lead to the realization of wearable,[22] skin-compatible,[23] implantable intelligent devices,[24] digestible smart electronics,[25] and novel biomemristors.[26]

Chitosan is one of the most efficient biocompatible natural solid polymer electrolyte (SPE) materials for humidity sensors,[27] ReRAMs, and memristors.[17,21,28−31] It can serve as a polymer matrix for nanomaterials' dispersion to produce nanocomposites.[21] For example, we have previously shown that a memristor based on gold-decorated chitosan presents more uniformity in both high- and low-resistance states compared to other chitosan-based biomemristors.[21]

Recently, carbon-based nanomaterials, such as carbon quantum dots (CQDs), have received significant attention in the research fields of biosensing,[32,33] bioimaging,[34] drug delivery,[35] photocatalysis,[36] and electrocatalysis[37] because of their unique properties of excellent water solubility and high luminescence.[38] The type of polymer matrix used is an essential factor that controls the distribution of carbon-based nanoparticles into the film and the electrical properties of the nanocomposites.[39] For example, it has been reported that the electrical properties of a nanocomposite comprising CQDs dispersed in an electronically inert polymer, such as polyvinyl alcohol (PVA), depend on the specific morphologies
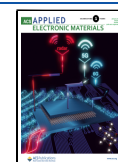
developed owing to the segregation of CQDs within the PVA polymer matrix.[39]

CQDs are research-attractive nanomaterials due to their tunability, high stability, large surface area, good electronic characteristics, catalytic activities, and low toxicity.[40] Herein, we present a biomemristor based on a CQD−chitosan nanocomposite. CQDs bind to the chitosan matrix via robust hydrogen bonds and electrostatic interconnections to form the CQD−chitosan nanocomposite.[41]

Chitosan has been effectively used in self-powered humidity sensors due to its swelling response to relative humidity.[27] Diffusion of the carbon nanomaterials in the SPE chitosan matrix is expected to improve the optical properties of the biopolymer by affecting the transmissive structural color of the produced nanocomposite. Furthermore, a CQD−chitosan nanocomposite has been employed as a cancer biomarker[42] and insulin aptasensor (biosensor).[43] The homogeneity of the CQD−chitosan nanocomposite and its high stability with good biocompatibility are desirable attributes for the SPE layer of a biomemristor.

Although the successful application of chitosan in bio-memristors has been previously reported,[17] improvements, including expanding the memory window, are required. In our previous reports, we have shown improved RS properties of pristine chitosan by doping Ag to its structure;[28,31] moreover, we have used a mixture of chitosan and starch to control the changes in the current level and realize a gradual switching behavior.[29] We have also confirmed uniform bipolar switching characteristics using Au−chitosan nanocomposites.[21]

In this study, we improve the switching properties of chitosan without sacrificing the thin film's transparency by integrating CQDs into the polymer structure. Furthermore, we increase the on/off ratio of the biomemristor to exceed 10^6. Finally, the 5 nm-sized CQDs dispersed in the chitosan matrix are suitable materials for filling the nanogaps of ∼10 nm toward further downscaling the memristive device.

A conventional biomemristor is a two-terminal device where a thin film of SPE is stacked between one inert and one active electrode in a vertical (sandwich) configuration. Alternatively, a nanogap-separated coplanar asymmetric architecture is more suitable than the vertical one due to its higher performance.[44] It has the potential to employ ultra-thin films, with their thickness defined by the nanogap channel length, and it can be easily integrated into static field-programmable gate arrays based on random-access memory.

In this report, we utilize adhesion lithography (a-Lith), a high-throughput, scalable, low-cost nanopatterning technique,[45] to produce asymmetric metal nanogaps and use them to fabricate biomemristors with a high on/off ratio. This fabrication procedure eliminates the requirement for expensive equipment and complex process steps involved in other patterning techniques, such as electron-beam lithography (EBL).[46] The successful reports of a-Lith fabricated nanogap electrodes have been demonstrated in high-frequency diodes,[47−50] fast-response speed photodetectors,[51] nanoscale polymer light-emitting diodes,[52] and flexible field-effect transistors.[53] Moreover, RS has been observed in empty Al−Al nanogap electrodes.[44] Multi-bit storage capabilities were obtained when carbon nanotubes dispersed in a polyfluorene matrix were deposited on top of these electrodes.[53] Ferro-electric tunnel junctions with ultra-high tunneling electro-resistance were demonstrated using the poly(vinylidene

fluoride-*co*-trifluoroethylene) [P(VDF-TrFE)] polymer and asymmetric coplanar Al−Au electrodes.[54]

This device is advantageous in several aspects over previously reported ones[55,56] and includes cost-effective and solution-assisted methods of the nanogap electrodes' nano-fabrication process without using costly and energy-consuming EBL techniques. Moreover, introducing CQDs with plenty of carbons to the chitosan matrix contributes to the improvement of RS properties by providing additional charge-trapping centers.

More specifically, this paper is an improvement over our previously published work in the following:

1 Improvement in the device structure:

The current work has two main superiorities compared to our previous biomemristors with coplanar structures.[57] First, it is scaled down from tens of micrometers to ∼15 nm, more than 3 orders of magnitude. Second, in most coplanar structures, both electrodes are made of the same material; here, we deposited two different electrodes separated by a 15 nm gap using a cost-effective nanofabrication technique without relying on expensive and time-consuming EBL.

2 Improvement in memory performance:

The on/off ratio represents an important figure of merit of memristive devices. A reliable memristor has an on/off ratio of at least 10. The more this number increases, the better the device performance is considered to be. A high on/off ratio is usually achieved by using complementary metal-oxide semi-conductor (CMOS)-compatible materials. Herein, we show an on/off ratio increase by 6 orders of magnitude upon using an alternative biocompatible material.

3 Improvement in the biocompatibility of the active material:

Using a natural polymer is the most crucial advantage of our suggested biomemristor due to its environmental-friendly nature and facile spin-coating method without using costly and energy-consuming high-vacuum-based deposition techni-ques.

4 Improvement in the conduction mechanism:

The addition of CQD in the chitosan matrix is beneficial for the conduction mechanism because CQDs employ a charge-trapping center, which has been thoroughly discussed in the conduction mechanism.

Here, we combine asymmetric nanogap electrodes com-posed of aluminum−gold with the solution-processable CQD−chitosan nanocomposite to produce biomemristors with a simple Al/CQD−chitosan/Au coplanar architecture. Furthermore, we elucidate the switching behavior of a natural CQD−chitosan-based SPE and explore its viability in biomemristive applications.

2. RESULTS AND DISCUSSION

2.1. Device Structure. Figure 1 shows the Au/CQD−chitosan/Al asymmetric coplanar structure of a nonvolatile biomemristor. Coplanar circular Al/Au electrodes, shown in the schematic in Figure 1a,b, were patterned via a-Lith on a 2 × 2 glass substrate. The steps of the a-Lith process are shown in the Supporting Information, Figure S1. In brief, after thermal evaporation and photolithography patterning of Al circular patterns on a glass substrate (Figure S1a), Al was functionalized with a self-assembled monolayer (SAM) (Figure
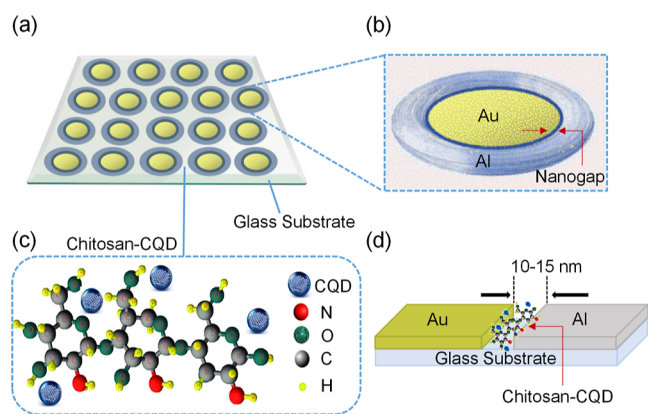
Figure 1. Schematic illustration of the (a) concentric circular memristor device structures with Al and Au electrodes of varying diameter; (b) zoomed-in area of a single device; (c) chemical structure of the nanocomposite biopolymer based on chitosan and CQDs; (d) cross-sectional device structure with the formed nanogap and the CQD−chitosan filling the space between the two electrodes.

S1b). Au was deposited via thermal evaporation after the SAM layer was attached to Al (Figure S1c). Then, an adhesive glue was applied on top of the Au and peeled off (Figure S1d). The Au over the SAM-functionalized Al region was removed upon peeling off the glue, leaving on the substrate coplanar Au and Al metals separated by a 10−15 nm gap (Figure S1e).

In common lateral (crossbar) RS memories, the device performance depends on the active layer's thickness. Here, the active layer is defined by the nanogap channel length. At the same time, the width of the electrodes may vary without changing the nanogap channel length (and consequently the active layer thickness in the coplanar geometry). More specifically, all devices have the same nanogap channel length (~15 nm), while the nanogap width is defined by the perimeter of the metals surrounding the nanogap. Therefore, the area of the flowing current is defined by the electrode thickness (40 nm) × the electrode length (here, it is 2500 μm).

Afterward, a CQD−chitosan (Figure 1c) nanocomposite solution of the SPE was spin-coated onto the fabricated electrodes and dried at 80 °C for 10 min. The nanogap between Al and Au was filled with the SPE solution (Figure 1d).

2.2. CQD−Chitosan Composite Film Characterization. The basic characteristic peaks of chitosan and the CQD−chitosan nanocomposite are shown in the Fourier transform infrared (FT-IR) spectra (Figure 2a). The significant peaks of chitosan at ~3370 and ~3295 cm^{-1} illustrate that the O−H and N−H stretching vibrations overlap. The ~2930 and ~2885 cm^{-1} peaks present the C−H stretching and 1660 cm^{-1} shows the N−H bending vibration. The basic peaks around 1080 cm^{-1} show the C−O stretch, including the primary and secondary hydroxyl groups, and the other peaks near 1000 cm^{-1} represent the bridge −O− stretch (Figure 2a).[58,59] The FT-IR spectrum of CQD−chitosan revealed the appearance of different peaks that correspond to functional groups located on the surface of CQDs, such as the stretching vibration of C−OH (3370 cm^{-1}), C−H (2920 cm^{-1}), and N−H (2800 cm^{-1}). Moreover, vibrational absorption bands matching C=O and C−O−C were recorded at 1650−1600 and 1400−1300 cm^{-1}, respectively.[58,59] The existence of −OH groups with their reducing activity on the surface of chitosan proved that
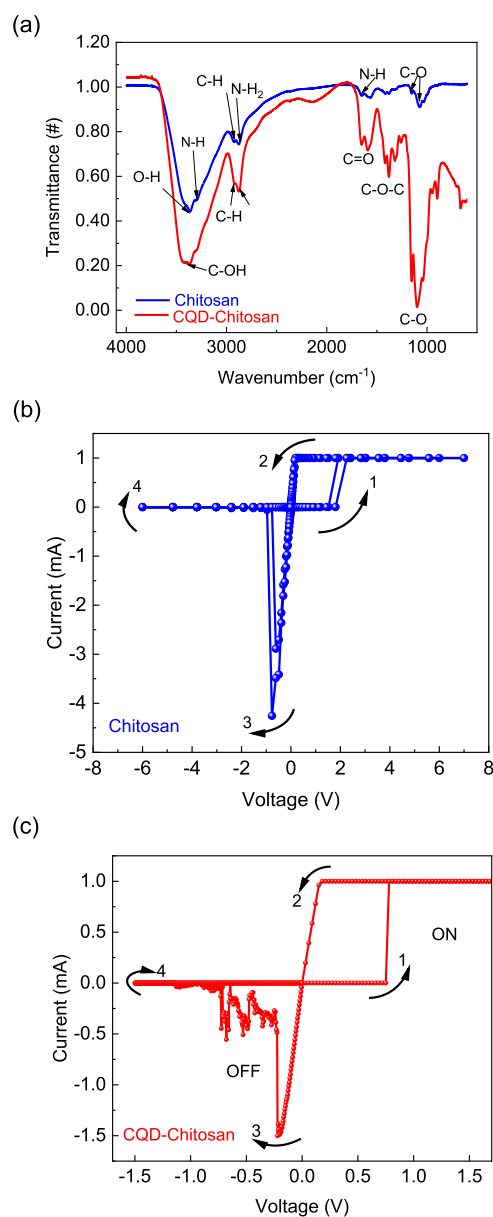

Figure 2. (a) FT-IR spectrum of a thin film of chitosan and the CQD−chitosan nanocomposite. (b) Linear I−V curves of a (c) biomemristive device with a pristine chitosan layer and a (c) CQD−chitosan layer in an Al/chitosan/Au coplanar biomemristor system with 1 mA current compliance; the arrows show the sweep direction.

chitosan can donate electrons during the formation reaction of the CQD−chitosan nanocomposite.[43,58]

2.3. Electrical Characterization. The current−voltage (I−V) characteristics of the pristine chitosan and the CQD−chitosan films were studied. Both chitosan-based biomemristors illustrated a typical RS behavior (Figure 2b,c). The chitosan-based device needs a forming voltage to trigger the RS memory effect (Figure S2a,b). Interestingly, the CQD−chitosan-based device works in a forming-free fashion. The biomemristor with the Al/CQD−chitosan/Au structure showed promise for lower power consumption since switching between the ON and OFF states could be controlled using a lower applied bias (Figure 2c). By measuring both types of biomemristors under a dc sweeping bias, the voltage range initially applied to the Al/chitosan/Au memristor was between
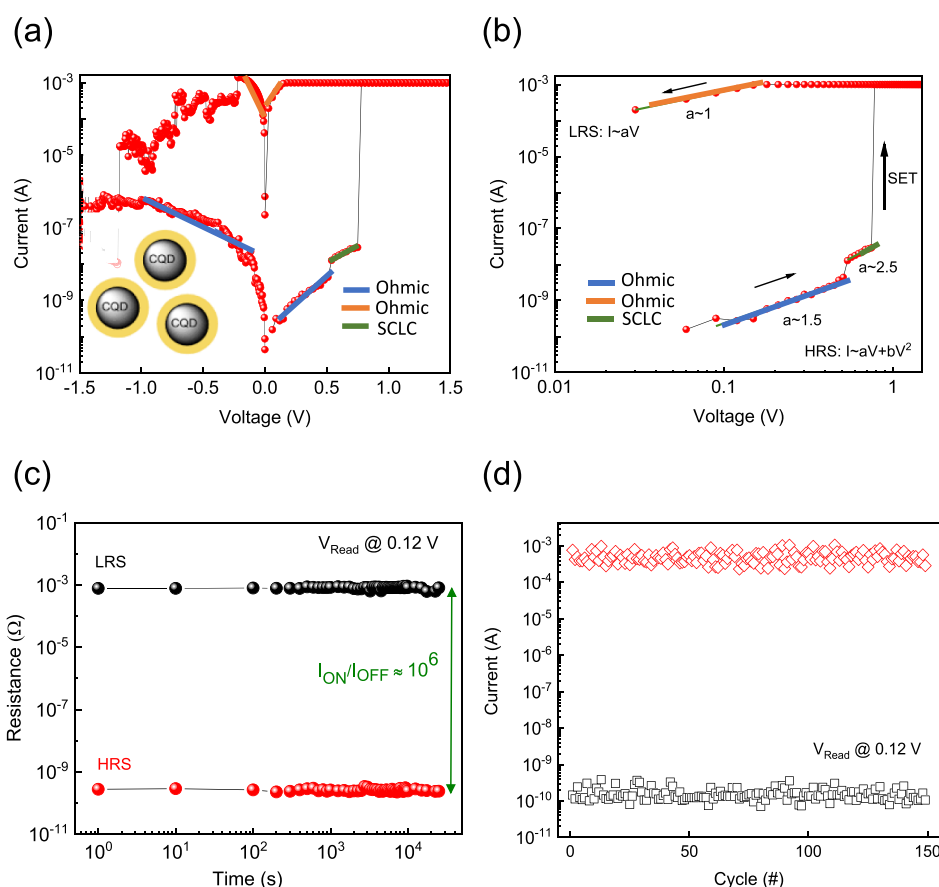
Figure 3. (a) Semilogarithmic and (b) double-logarithmic $I-V$ curve of Al/CQD−chitosan/Au biomemristor with the coplanar structure under positive and negative voltage regions (inset). (c) Data retention properties of the LRS and HRS states under continuous reading voltage at room temperature. (d) Endurance characteristics of the device for 150 cycles under applying 0.12 V.

±6 V, with a $V_{set} \sim 1.6$ V (Figure 2b). However, the device with the CQD−chitosan SPE worked under ±1.6 V with a $V_{set} \sim 0.75$ V (Figure 2c).

Since Al is a reactive metal, oxidation is inevitable when exposed to an ambient environment, where it forms a thin layer (*ca.* 1 nm) of Al_2O_3 on its surface.[54] Therefore, a slightly higher potential may be required to form the initial conductive filament (CF) due to the presence of this native Al_2O_3 layer.[60] Although currents can tunnel through such a thin layer, compared with the SPE layer, it is too thin to contribute considerably to the switching mechanism.

By assimilation of CQDs to the chitosan matrix, the produced charge trapping centers enhance the switching mechanism. Compared to the Au−chitosan nanocomposites in a crossbar structure, the on/off ratio is improved by more than 5 orders of magnitude, and the set/reset voltage is reduced to half.[21] A perfect bipolar RS cycle (including ON and OFF states) was determined to identify the CF formation and rupture in the SPE (Figure 2c).

This is better depicted in the semilogarithmic plot of the same device, shown in Figure 3a.

During the first voltage sweep from 0 to V_{set}, the Al electrode is oxidized to Al^{3+}, and the Al cations create a CF near the Au inert electrode by reducing to Al atoms. After forming the CF, the biomemristor reaches its low resistant state (LRS) or ON state. We applied a 1 mA compliance current to prevent the permanent breakdown of the biomemristor. Subsequently, by changing the polarity of the applied voltage, the CF is

ruptured, and the memory device reaches back to its pristine state with a high resistant state (HRS) or OFF state (Figure 3a).

To further elucidate the conduction mechanism of the coplanar memristive device, we replotted and analyzed the double-logarithmic $I-V$ curves of the CQD−chitosan-based biomemristor upon applying the sweeping cycle $0 \rightarrow 1.6 \rightarrow 0 \rightarrow -1.6 \rightarrow 0$ V to the Al active electrode, while Au was grounded (Figure 3b, Supporting Information; Figure S3). The $I-V$ characteristics give evidence of the RS transition from trap-assisted space-charge-limited conduction (SCLC) to a CF formation, as is indicated by the characteristics in both semi- and double-logarithmic plots (Figure 3a,b). More specifically, the linear fit of the log−log plot at the HRS regime illustrates that the current conduction in the SPE layer of the biomemristor obeys the SCLC mechanism. The conduction behavior in the trap-controlled SCLC is represented by a square-law dependency on voltage (eq 1)

$$J = \frac{9\varepsilon_0\varepsilon_r\mu V^2}{8d^3}\Theta \tag{1}$$

where J [A/cm^2] is the current density, μ [cm^2/V·s] is the carrier mobility, ε_0 [F/m] is the permittivity of space, ε_r is the static dielectric constant, d [cm] is the thickness of the thin film, Θ is the ratio of the carrier density to the total carrier, and V [V] is the applied voltage.[61−63] SCLC is, thus, governed by traps and the ratio of the free careers to the trapped ones.[28,64] The SCLC mechanism, in this case, happens owing to the traps

generated by adding CQDs in the chitosan structure in the nanocomposite SPE layer.

There are two representative sections in the $0 \rightarrow 1.6$ V of the HRS regime; the $I-V$ curve is almost linear at the lower voltage section ($0 \rightarrow 0.51$ V) (Figure 3b). At the higher voltage section ($0.51 \rightarrow 0.75$ V), the curve changed to a quadratic line with a slope of 2.5 before reaching the V_{set}. This may be explained as follows: At first, when the voltage is low (0 V $< V < 0.51$ V), the electric field is not high enough to inject electrical charges into the SPE layer. The amount of injected charge carriers is lower than the amount of thermally produced ones, compatible with Ohm's law ($I \propto V$).[28] With gradually increasing voltage, the traps are partially filled by the transferred charges from chitosan to the CQDs. Because the trap density is higher than the free charge carriers, the charge trapping phenomenon occurs. When the voltage is increased, the overflowing charge carriers fill the generated trap centers by CQDs. Completely filled traps lead to a higher electron concentration in the SPE layer of the biomemristor. Approaching the operating voltage increases the amount of the injected charge carriers exponentially, and electrons conduct through the CF.[65]

HRS's conduction mechanism displays a square law dependency on the applied voltage ($I \propto V^2$), following eq 1. The traps and the ratio of the unoccupied charge carriers to the trapped ones control the SCLC mechanism.[28,66]

By sweeping the voltage from $1.6 \rightarrow 0$ V, the $I-V$ measurement showed a linear behavior of $I \propto V$, which is consistent with the filamentary conduction path (Figure 3a,b). Ohm's law is the prevalent process in this LRS region (eq 2)

$$J_{Ohm} = qn_0\mu\frac{V}{d} \tag{2}$$

where q is the charge magnitude and n_0 is the intrinsic charge density; considering the logarithm of the above equation, a linear relationship between J and V is achieved.[63]

Changing the bias to a negative voltage sweep, the double-logarithmic $I-V$ curve from $0 \rightarrow -1.6$ and $-1.6 \rightarrow 0$ V was similar to the $1.6 \rightarrow 0$ V region obeying Ohmic conduction (Supporting Information, Figure S3). By reversing the bias polarity, the charges in the traps are neutralized and detrapped. While rupturing the CF, the internal electric field decreases by the applied electric voltage, and the device returns to its off state.

We further evaluated the memristive performance of the Al/CQD−chitosan/Au device by recording the retention characteristics for both the LRS and HRS states at a reading bias of 0.12 V. The biomemristor showed a high on/off ratio of ~10^6 without any appreciable degradation in the LRS and HRS for 3 h (Figure 3c). Endurance characteristics completed the memristive reliability test; both LRS and HRS were stable without failure for up to 150 cycles of biasing under a 0.12 V read voltage. Therefore, we concluded that the Al/CQD−chitosan/Au device is a reliable and reproducible biomemristor. To realize the advantages of the CQD−chitosan-based coplanar memristor, we compare our suggested memory device with previous studies on chitosan-based memristors (Supporting Information, Table S1).

2.4. RS Mechanism. The RS mechanism of the Al/CQD−chitosan/Au device can be explained via CF formation/rupture theory (Figure 4). By applying a positive bias voltage to the active electrode, Al^{3+} cations move toward the Au. We consider the biomemristor as a solid-state electrochemical metallization
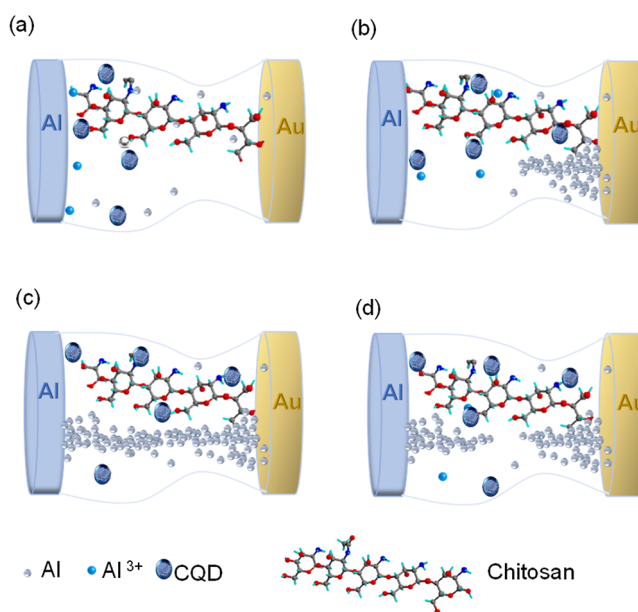

Figure 4. Proposed RS mechanism: (a,b) Al^{3+} ion movement under positive voltage; gradually reducing Al^{3+} near the Au inert electrode and carbons of CQDs together; (c) formation of an Al CF to make a path that bridges Al and Au electrodes; and (d) rupture of the created filaments by reversing the voltage polarity.

(ECM) cell; therefore, Al and Au serve as the anode and the cathode of the ECM. The anodic dissolution happens between Al and CQD−chitosan, the cell's SPE layer (Al $\rightarrow$ Al^{3+} + $3e^-$).[66] When the electric field is high enough, Al^{3+} cations penetrate the SPE and transfer toward Au (Figure 4a). Because CQDs are not as active as Al^{3+}, they slowly diffuse into the SPE, being more ordered than Al cations.

Meanwhile, a group of carbon cluster ions moves toward the cathode electrode under an electric field.[67] The distributed CQDs inside the SPE might serve as electron-trapping centers. They are responsible for the conduction mechanism by enhancing the localized electric field to accumulate electrons.[68]

Since the CF is proposed as the predominant switching mechanism, we postulate the RS phenomenon to be attributed to a metallic CF based on Al atoms. More specifically, because Au is in charge of the cathodic reaction, the dispersed Al^{3+} cations inside the SPE are reduced to Al atoms (Al^{3+} + $3e^- \rightarrow$ Al). The reduced Al atoms are electrochemically deposited on the interface of the SPE and the Au electrode and create Al filaments (Figure 4b).

Therefore, a CF of Al atoms is created between Al and Au as a connection path between the anode and cathode of the device (Figure 4c).

This process is similar to a short circuit in a conventional electrochemical cell called the ON state. After the formation of the CF, the applied voltage decreases due to the current compliance, which prevents the deposition of extra Al atoms that would lead to the permanent breakdown of the biomemristor.[31] The device was switched to its pristine state by applying an appropriate negative voltage. The cations migrated toward the Au electrode and were reduced to Al atoms, leading the device to return to its original HRS state (Al^{3+} + $3e^- \rightarrow$ Al). Therefore, the rupture of the CF happens by applying a successive negative voltage, which causes a break in the narrowest part of the CF (Figure 4d). Our biomemristor demonstrated a reproducible resistance change behavior by

applying a sufficient electrical voltage due to the building and rupture of the CF.

3. CONCLUSIONS

We introduced a nanocomposite of CQD−chitosan as a sustainable RS layer of a biomemristor. We employed this material to successfully demonstrate a biomemristor in a coplanar device structure using the facile method of a-Lith to produce the nanogap coplanar electrodes. This memory device is an attractive candidate for environmentally benign and cost-effective innovative nanoelectronics. We showed the resistance change characteristics of the CQD−chitosan memristive device with bipolar properties for future nonvolatile memories. The biomemristor showed a high on/off ratio of 10^6 and a data retention of 10^4 s. It is suggested that the formation and disruption of CF are responsible for the switching characteristics. The coplanar structure of the device favors the facile device fabrication using solution-based processes at low temperatures, fully compatible with flexible substrates. This study reveals that memristors based on bioinspired nanocomposites can enable biocompatible, transparent, and green nonvolatile memory devices (ReRAM).

4. METHODS

4.1. Nanogap Memristive Device Fabrication. Using a-Lith, we patterned asymmetric arrays of Al and Au nanogap electrodes on glass substrates (Figure S1). At first, we ultrasonically cleaned a 2 × 2 cm glass substrate using deionized water, acetone, and isopropanol for 10 min and then dried it with an N_2 gun. Then, we loaded the cleaned substrate into a high vacuum (10^{-6} mbar) thermal evaporator system and deposited a 40 nm thick Al electrode. We patterned the circles with conventional photolithography followed by a wet etching process of Al. To make a hydrophobic surface by forming a SAM on the Al electrode, we immersed the patterned glass substrates in a 1 mM octadecyl phosphonic acid solution (Sigma-Aldrich). Then, we thermally deposited a 35 nm Au electrode with a 5 nm Al as an adhesion layer on the glass substrate. Next, we coated an adhesive film (First Contact, Photonic Cleaning Technologies) on the substrate using a brush and air-dried it for 20 min. A tape was used to peel off the adhesive glue to remove the Au metal from the top part of the SAM-coated Al electrode. We performed additional photolithography and wet etching steps to separate each memristor from the patterned Al electrode. Finally, we removed the residual photoresist and SAM via ultraviolet-ozone cleaning, and, eventually, empty nanogaps were created.

4.2. Deposition of a Solution-Processed Thin Film. We prepared the SPE solution using deacetylated chitosan powder (deacetylation degree 75−85%, Sigma-Aldrich). We dissolved the powders in a diluted acetic acid solution (1%) followed by 0.22 μm polyvinylidene fluoride filters (Whatman) to make a clear and transparent solution. Next, we prepared a water-soluble CQD−chitosan nanocomposite by mixing the CQD solution (Sigma-Aldrich) with chitosan in a 1:1 volume ratio under 5 min magnetic stirring. We spin-coated the as-prepared mixed solution on the nanogap patterned transparent substrate at 1000 rpm for 5 s and 3000 rpm for 60 s and then heated it at 80 °C for 10 min on a hotplate. After drying the spin-coated thin film, the nanogap is filled with the CQD−chitosan nanocomposite, and our coplanar device bears an Al/CQD−chitosan/Au structure.

4.3. Electrical Characterizations. The electrical characteristics of the biomemristors were measured in two-terminal configurations under ambient temperature using a semiconductor parameter analyzer [Keysight (Agilent), B1500A] for applying the voltage and measuring current. The sample was placed in a probe station during all the measurements, and bias voltages were applied to the outer circular electrode (Al), while the inner circular electrode (Au) was grounded.

4.4. FT-IR Analysis. All FT-IR analyses were performed using a Bruker Tensor 37 with Hyperiom 2000 IR microscope (USA). For the analysis, the CQD−chitosan solution was spin-coated on a gold substrate, and the measurement range was between 400 and 4000 cm^{-1}.

■ ASSOCIATED CONTENT

⑤ Supporting Information

The Supporting Information is available free of charge at https://pubs.acs.org/doi/10.1021/acsaelm.2c00979.

> All the data of Supporting Information is available online step-by-step fabrication procedures of nanogap electrodes; $I-V$ curves of the pristine device and the forming voltage of the Au/chitosan/Al memristive device; log−log $I-V$ curve of a biomemristor (negative region); and comparison of previous studies on chitosan-based memristors with this report (PDF)

■ AUTHOR INFORMATION

Corresponding Author

Niloufar Raeis-Hosseini − *Department of Electronics and Electrical Engineering, Imperial College London, London SW7 2BT, U.K.;* ⓞ orcid.org/0000-0002-3234-9544; Email: n.raeishosseini@imperial.ac.uk, nraeis@cranfield.ac.uk

Authors

Dimitra G. Georgiadou − *Electronics and Computer Science, University of Southampton, Southampton SO17 1BJ, U.K.;* ⓞ orcid.org/0000-0002-2620-3346

Christos Papavassiliou − *Department of Electronics and Electrical Engineering, Imperial College London, London SW7 2BT, U.K.*

Complete contact information is available at: https://pubs.acs.org/10.1021/acsaelm.2c00979

Notes

The authors declare no competing financial interest.

■ ACKNOWLEDGMENTS

■ REFERENCES

(1) Wu, L.; Wang, A.; Shi, J.; Yan, J.; Zhou, Z.; Bian, C.; Ma, J.; Ma, R.; Liu, H.; Chen, J.; Huang, Y.; Zhou, W.; Bao, L.; Ouyang, M.; Pennycook, S. J.; Pantelides, S. T.; Gao, H.-J. Atomically sharp interface enabled ultrahigh-speed non-volatile memory devices. *Nat. Nanotechnol.* **2021**, *16*, 882−887.

(2) Zhou, G.; Wang, Z.; Sun, B.; Zhou, F.; Sun, L.; Zhao, H.; Hu, X.; Peng, X.; Yan, J.; Wang, H.; Wang, W.; Li, J.; Yan, B.; Kuang, D.; Wang, Y.; Wang, L.; Duan, S. Volatile and Nonvolatile Memristive Devices for Neuromorphic Computing. *Adv. Electron. Mater.* **2022**, *8*, 2101127.

(3) Kumar, P.; Zhu, K.; Gao, X.; Wang, S.-D.; Lanza, M.; Thakur, C. S. Hybrid architecture based on two-dimensional memristor crossbar array and CMOS integrated circuit for edge computing. *npj 2D Mater. Appl.* **2022**, *6*, 8.

(4) Kim, K.-H.; Gaba, S.; Wheeler, D.; Cruz-Albrecht, J. M.; Hussain, T.; Srinivasa, N.; Lu, W. A functional hybrid memristor crossbar-array/CMOS system for data storage and neuromorphic applications. *Nano Lett.* **2012**, *12*, 389−395.

(5) Yao, P.; Wu, H.; Gao, B.; Tang, J.; Zhang, Q.; Zhang, W.; Yang, J. J.; Qian, H. Fully hardware-implemented memristor convolutional neural network. *Nature* **2020**, *577*, 641−646.

(6) Lin, P.; Li, C.; Wang, Z.; Li, Y.; Jiang, H.; Song, W.; Rao, M.; Zhuo, Y.; Upadhyay, N. K.; Barnell, M.; Wu, Q.; Yang, J. J.; Xia, Q. Three-dimensional memristor circuits as complex neural networks. *Nat. Electron.* **2020**, *3*, 225−232.

(7) Cai, H.; Guo, Y.; Liu, B.; Zhou, M.; Chen, J.; Liu, X.; Yang, J. Proposal of Analog In-Memory Computing With Magnified Tunnel Magnetoresistance Ratio and Universal STT-MRAM Cell. *IEEE Trans. Circuits Syst. I Regul. Pap.* **2022**, *69*, 1519−1531.

(8) Raeis-Hosseini, N.; Rho, J. Dual-Functional Nanoscale Devices Using Phase-Change Materials: A Reconfigurable Perfect Absorber with Nonvolatile Resistance-Change Memory Characteristics. *Appl. Sci.* **2019**, *9*, 564.

(9) Raeis-Hosseini, N.; Lim, S.; Hwang, H.; Rho, J. Reliable Ge2Sb2Te5-Integrated high-density nanoscale conductive bridge random access memory using facile nitrogen-doping strategy. *Adv. Electron. Mater.* **2018**, *4*, 1800360.

(10) Raeis-Hosseini, N.; Rho, J. Metasurfaces based on phase-change material as a reconfigurable platform for multifunctional devices. *Materials* **2017**, *10*, 1046.

(11) Pickett, M. D.; Medeiros-Ribeiro, G.; Williams, R. S. A scalable neuristor built with Mott memristors. *Nat. Mater.* **2013**, *12*, 114−117.

(12) Lee, M.-J.; Lee, C. B.; Lee, D.; Lee, S. R.; Chang, M.; Hur, J. H.; Kim, Y.-B.; Kim, C.-J.; Seo, D. H.; Seo, S.; Chung, U.-I.; Yoo, I.-K.; Kim, K. A fast, high-endurance and scalable non-volatile memory device made from asymmetric Ta2O5−x/TaO2−x bilayer structures. *Nat. Mater.* **2011**, *10*, 625−630.

(13) Valov, I.; Linn, E.; Tappertzhofen, S.; Schmelzer, S.; van den Hurk, J.; Lentz, F.; Waser, R. Nanobatteries in redox-based resistive switches require extension of memristor theory. *Nat. Commun.* **2013**, *4*, 1771.

(14) Yin, L.; Cheng, R.; Wen, Y.; Zhai, B.; Jiang, J.; Wang, H.; Liu, C.; He, J. High-Performance Memristors Based on Ultrathin 2D Copper Chalcogenides. *Adv. Mater.* **2022**, *34*, 2108313.

(15) Luo, Z.; Wang, Z.; Guan, Z.; Ma, C.; Zhao, L.; Liu, C.; Sun, H.; Wang, H.; Lin, Y.; Jin, X. High-precision and linear weight updates by subnanosecond pulses in ferroelectric tunnel junction for neuro-inspired computing. *Nat. Commun.* **2022**, *13*, 699.

(16) Marković, D. Synchronization by memristors. *Nat. Mater.* **2022**, *21*, 4−5.

(17) Raeis-Hosseini, N.; Lee, J.-S. Resistive switching memory using biomaterials. *J. Electroceram.* **2017**, *39*, 223−238.

(18) Hennen, T.; Wichmann, E.; Waser, R.; Wouters, D.; Bedau, D. Stabilizing amplifier with a programmable load line for characterization of nanodevices with negative differential resistance. *Rev. Sci. Instrum.* **2022**, *93*, 024705.

(19) von Witzleben, M.; Wiefels, S.; Kindsmüller, A.; Stasner, P.; Berg, F.; Cüppers, F.; Hoffmann-Eifert, S.; Waser, R.; Menzel, S.; Böttger, U. Intrinsic RESET speed limit of valence change memories. *ACS Appl. Electron. Mater.* **2021**, *3*, 5563−5572.

(20) Arunagirinathan, R. N.; Meher, N.; Iyer, P. K. Self-Assembled Naphthalimide Nanoparticles for Nonvolatile ReRAM Devices: An Efficient Approach toward High Performance Solution-Processed and All-Organic Two-Terminal Resistive Memory Devices. *ACS Appl. Electron. Mater.* **2019**, *1*, 2437−2444.

(21) Raeis-Hosseini, N.; Rho, J. Solution-processed flexible biomemristor based on gold-decorated chitosan. *ACS Appl. Mater. Interfaces* **2021**, *13*, 5445−5450.

(22) Cima, M. J. Next-generation wearable electronics. *Nat. Biotechnol.* **2014**, *32*, 642−643.

(23) Ditte, K.; Perez, J.; Chae, S.; Hambsch, M.; Al-Hussein, M.; Komber, H.; Formanek, P.; Mannsfeld, S. C.; Fery, A.; Kiriy, A.; Lissel, F. Ultrasoft and High-Mobility Block Copolymers for Skin-Compatible Electronics. *Adv. Mater.* **2021**, *33*, 2005416.

(24) Song, Y.; Min, J.; Gao, W. Wearable and implantable electronics: moving toward precision therapy. *ACS Nano* **2019**, *13*, 12280−12286.

(25) Lanzani, G. Organic electronics meets biology. *Nat. Mater.* **2014**, *13*, 775−776.

(26) Sun, B.; Zhou, G.; Guo, T.; Zhou, Y. N.; Wu, Y. A. Biomemristors as the next generation bioelectronics. *Nano Energy* **2020**, *75*, 104938.

(27) Jang, J.; Kang, K.; Raeis-Hosseini, N.; Ismukhanova, A.; Jeong, H.; Jung, C.; Kim, B.; Lee, J. Y.; Park, I.; Rho, J. Self-Powered Humidity Sensor Using Chitosan-Based Plasmonic Metal-Hydrogel-Metal Filters. *Adv. Opt. Mater.* **2020**, *8*, 1901932.

(28) Hosseini, N. R.; Lee, J. S. Biocompatible and Flexible Chitosan-Based Resistive Switching Memory with Magnesium Electrodes. *Adv. Funct. Mater.* **2015**, *25*, 5586−5592.

(29) Raeis-Hosseini, N.; Lee, J.-S. Controlling the Resistive Switching Behavior in Starch-Based Flexible Biomemristors. *ACS Appl. Mater. Interfaces* **2016**, *8*, 7326−7332.

(30) Raeis-Hosseini, N.; Park, Y.; Lee, J. S. Flexible Artificial Synaptic Devices Based on Collagen from Fish Protein with Spike-Timing-Dependent Plasticity. *Adv. Funct. Mater.* **2018**, *28*, 1800553.

(31) Raeis Hosseini, N.; Lee, J.-S. Resistive Switching Memory Based on Bioinspired Natural Solid Polymer Electrolytes. *ACS Nano* **2014**, *9*, 419−426.

(32) Buk, V.; Pemble, M. E. A highly sensitive glucose biosensor based on a micro disk array electrode design modified with carbon quantum dots and gold nanoparticles. *Electrochim. Acta* **2019**, *298*, 97−105.

(33) Li, H.; Yan, X.; Qiao, S.; Lu, G.; Su, X. Yellow-emissive carbon dot-based optical sensing platforms: cell imaging and analytical applications for biocatalytic reactions. *ACS Appl. Mater. Interfaces* **2018**, *10*, 7737−7744.

(34) Cao, L.; Wang, X.; Meziani, M. J.; Lu, F.; Wang, H.; Luo, P. G.; Lin, Y.; Harruff, B. A.; Veca, L. M.; Murray, D.; Xie, S.-Y.; Sun, Y.-P. Carbon dots for multiphoton bioimaging. *J. Am. Chem. Soc.* **2007**, *129*, 11318−11319.

(35) Dong, J.; Wang, K.; Sun, L.; Sun, B.; Yang, M.; Chen, H.; Wang, Y.; Sun, J.; Dong, L. Application of graphene quantum dots for simultaneous fluorescence imaging and tumor-targeted drug delivery. *Sens. Actuators, B* **2018**, *256*, 616−623.

(36) Fernando, K. S.; Sahu, S.; Liu, Y.; Lewis, W. K.; Guliants, E. A.; Jafariyan, A.; Wang, P.; Bunker, C. E.; Sun, Y.-P. Carbon quantum dots and applications in photocatalytic energy conversion. *ACS Appl. Mater. Interfaces* **2015**, *7*, 8363−8376.

(37) Amini, N.; Gholivand, M. B.; Shamsipur, M. Electrocatalytic determination of traces of insulin using a novel silica nanoparticles-Nafion modified glassy carbon electrode. *J. Electroanal. Chem.* **2014**, *714*−*715*, 70−75.

(38) Wang, Y.; Hu, A. Carbon quantum dots: synthesis, properties and applications. *J. Mater. Chem. C* **2014**, *2*, 6921−6939.

(39) Ambasankar, K.; Bhattacharjee, L.; Jat, S. K.; Bhattacharjee, R. R.; Mohanta, K. Study of Electrical Charge Storage in Polymer-Carbon Quantum Dot Composite. *ChemistrySelect* **2017**, *2*, 4241−4247.

(40) Amini, N.; Shamsipur, M.; Gholivand, M. B.; Barati, A. A glassy carbon electrode modified with carbon quantum dots and polyalizarin yellow R dyes for enhanced electrocatalytic oxidation and nanomolar detection of L-cysteine. *Microchem. J.* **2017**, *131*, 9−14.

(41) Yan, Z.; Yang, X.; Hua, Y.; Li, Z.; Liu, Y.; Lin, Y. An impedance sensor based on chitosan-carbon quantum dots for the detection sialic acid in humuan serum. *Microchem. J.* **2021**, *169*, 106520.

(42) Mansur, A. A.; Mansur, H. S.; Soriano-Araújo, A.; Lobato, Z. I. Fluorescent Nanohybrids Based on Quantum Dot-Chitosan-Antibody as Potential Cancer Biomarkers. *ACS Appl. Mater. Interfaces* **2014**, *6*, 11403−11412.

(43) Abazar, F.; Noorbakhsh, A. Chitosan-carbon quantum dots as a new platform for highly sensitive insulin impedimetric aptasensor. *Sens. Actuators, B* **2020**, *304*, 127281.

(44) Semple, J.; Wyatt-Moon, G.; Georgiadou, D. G.; McLachlan, M. A.; Anthopoulos, T. D. Semiconductor-free nonvolatile resistive switching memory devices based on metal nanogaps fabricated on

flexible substrates via adhesion lithography. *IEEE Trans. Electron Devices* **2017**, *64*, 1973−1980.

(45) Beesley, D. J.; Semple, J.; Krishnan Jagadamma, L.; Amassian, A.; McLachlan, M. A.; Anthopoulos, T. D.; deMello, J. C. Sub-15-nm patterning of asymmetric metal electrodes and devices by adhesion lithography. *Nat. Commun.* **2014**, *5*, 3933.

(46) Manheller, M.; Trellenkamp, S.; Waser, R.; Karthäuser, S. Reliable fabrication of 3 nm gaps between nanoelectrodes by electron-beam lithography. *Nanotechnology* **2012**, *23*, 125302.

(47) Semple, J.; Rossbauer, S.; Anthopoulos, T. D. Analysis of Schottky contact formation in coplanar Au/ZnO/Al nanogap radio frequency diodes processed from solution at low temperature. *ACS Appl. Mater. Interfaces* **2016**, *8*, 23167−23174.

(48) Semple, J.; Rossbauer, S.; Burgess, C. H.; Zhao, K.; Jagadamma, L. K.; Amassian, A.; McLachlan, M. A.; Anthopoulos, T. D. Radio frequency coplanar ZnO Schottky nanodiodes processed from solution on plastic substrates. *Small* **2016**, *12*, 1993−2000.

(49) Georgiadou, D. G.; Semple, J.; Anthopoulos, T. D.Adhesion Lithography for Fabrication of Printed Radio-Frequency Diodes. *SPIE Newsroom*; SPIE, 2017.

(50) Georgiadou, D. G.; Semple, J.; Sagade, A. A.; Forstén, H.; Rantakari, P.; Lin, Y.-H.; Alkhalil, F.; Seitkhan, A.; Loganathan, K.; Faber, H. 100 GHz zinc oxide Schottky diodes processed from solution on a wafer scale. *Nat. Electron.* **2020**, *3*, 718−725.

(51) Georgiadou, D. G.; Lin, Y. H.; Lim, J.; Ratnasingham, S.; McLachlan, M. A.; Snaith, H. J.; Anthopoulos, T. D. High responsivity and response speed single-layer mixed-cation lead mixed-halide perovskite photodetectors based on nanogap electrodes manufactured on large-area rigid and flexible substrates. *Adv. Funct. Mater.* **2019**, *29*, 1901371.

(52) Wyatt-Moon, G.; Georgiadou, D. G.; Zoladek-Lemanczyk, A.; Castro, F. A.; Anthopoulos, T. D. Flexible nanogap polymer light-emitting diodes fabricated via adhesion lithography (a-Lith). *J. Phys.: Mater.* **2018**, *1*, 01LT01.

(53) Semple, J.; Georgiadou, D. G.; Wyatt-Moon, G.; Yoon, M.; Seitkhan, A.; Yengel, E.; Rossbauer, S.; Bottacchi, F.; McLachlan, M. A.; Bradley, D. D. Large-area plastic nanogap electronics enabled by adhesion lithography. *npj Flexible Electron.* **2018**, *2*, 18.

(54) Kumar, M.; Georgiadou, D. G.; Seitkhan, A.; Loganathan, K.; Yengel, E.; Faber, H.; Naphade, D.; Basu, A.; Anthopoulos, T. D.; Asadi, K. Colossal tunneling electroresistance in co-planar polymer ferroelectric tunnel junctions. *Adv. Electron. Mater.* **2020**, *6*, 1901091.

(55) Meng, F.; Sana, B.; Li, Y.; Liu, Y.; Lim, S.; Chen, X. Bioengineered tunable memristor based on protein nanocage. *Small* **2014**, *10*, 277−283.

(56) He, C.; Shi, Z.; Zhang, L.; Yang, W.; Yang, R.; Shi, D.; Zhang, G. Multilevel resistive switching in planar graphene/SiO2 nanogap structures. *ACS Nano* **2012**, *6*, 4214−4221.

(57) Hosseini, N. R.; Lee, J. S. Biocompatible and Flexible Chitosan-Based Resistive Switching Memory with Magnesium Electrodes. *Adv. Funct. Mater.* **2015**, *25*, 5586−5592.

(58) Brugnerotto, J.; Lizardi, J.; Goycoolea, F.; Argüelles-Monal, W.; Desbrieres, J.; Rinaudo, M. An infrared investigation in relation with chitin and chitosan characterization. *Polymer* **2001**, *42*, 3569−3580.

(59) Wang, X.; Tang, R.; Zhang, Y.; Yu, Z.; Qi, C. Preparation of a novel chitosan based biopolymer dye and application in wood dyeing. *Polymers* **2016**, *8*, 338.

(60) Gale, E.; Mayne, R.; Adamatzky, A.; de Lacy Costello, B. Drop-coated titanium dioxide memristors. *Mater. Chem. Phys.* **2014**, *143*, 524−529.

(61) Pan, F.; Chen, C.; Wang, Z.-s.; Yang, Y.-c.; Jing, Y.; Fei, Z. Nonvolatile resistive switching memories-characteristics, mechanisms and challenges. *Prog. Nat. Sci.: Mater. Int.* **2010**, *20*, 1−15.

(62) Prajitha, K. P.; Chithiravel, S.; Krishnamoorthy, K.; Asha, S. K. Structure−property relationship in charge transporting behaviour of room temperature liquid crystalline perylenebisimides. *J. Mater. Chem. C* **2014**, *2*, 9882−9891.

(63) Tayeb, I. A.; Zhao, F.; Abdullah, J. M.; Cheong, K. Y. Resistive switching behaviour in a polymannose film for multistate non-volatile memory application. *J. Mater. Chem. C* **2021**, *9*, 1437−1450.

(64) Tran, K. M.; Do, D. P.; Thi, K. H. T.; Pham, N. K. Influence of top electrode on resistive switching effect of chitosan thin films. *J. Mater. Res.* **2019**, *34*, 3899−3906.

(65) Zhang, P.; Xu, B.; Gao, C.; Chen, G.; Gao, M. Facile synthesis of Co9Se8 quantum dots as charge traps for flexible organic resistive switching memory device. *ACS Appl. Mater. Interfaces* **2016**, *8*, 30336−30343.

(66) Valov, I.; Lu, W. D. Nanoscale electrochemistry using dielectric thin films as solid electrolytes. *Nanoscale* **2016**, *8*, 13828−13837.

(67) Pei, Y.; Zhou, Z.; Chen, A. P.; Chen, J.; Yan, X. A carbon-based memristor design for associative learning activities and neuromorphic computing. *Nanoscale* **2020**, *12*, 13531−13539.

(68) Zeng, T.; Yang, Z.; Liang, J.; Lin, Y.; Cheng, Y.; Hu, X.; Zhao, X.; Wang, Z.; Xu, H.; Liu, Y. Flexible and transparent memristive synapse based on polyvinylpyrrolidone/N-doped carbon quantum dot nanocomposites for neuromorphic computing. *Nanoscale Adv.* **2021**, *3*, 2623−2631.